PHYSICAL REVIEW A **111**, 043112 (2025)

Radiative cooling of the deprotonated cyan fluorescent protein chromophore anion

James Flotte de Pouzols,[1] Arun Subramani,[2] Eleanor K. Ashworth,[3] James N. Bull,[3] Henrik Cederquist,[2]
Jordan Dezalay,[2,4] Nanna Holmgaard List,[5] Paul Martini,[2] José E. Navarro Navarrete,[2] Henning T. Schmidt,[2]
Henning Zettergren,[2] Boxing Zhu,[2] and Mark H. Stockett[2,*]
[1]*Department of Chemistry, Université Paris-Saclay, Gif-sur-Yvette, France*
[2]*Department of Physics, Stockholm University, Stockholm, Sweden*
[3]*Chemistry, Faculty of Science, University of East Anglia, Norwich, United Kingdom*
[4]*Department of Physics, Aix-Marseille Université, Marseille, France*
[5]*Department of Chemistry, KTH Royal Institute of Technology, Stockholm, Sweden*

(Received 10 January 2025; accepted 9 April 2025; published 18 April 2025)

An electrospray ion source has been coupled to a cryogenic electrostatic ion-beam storage ring to enable experimental studies of the fundamental properties of biomolecular ions and their reactions in the gas phase on longer timescales than with previous instruments. Using this equipment, we have measured the vibrational radiative cooling rate of the deprotonated anion of the chromophore of the cyan fluorescent protein, a color-shifted mutant of the iconic green fluorescent protein. Time-resolved dissociation rates of collisionally activated ions are first measured to benchmark a model of the dissociation rate coefficient. Storage time-dependent laser-induced dissociation rates are then measured to probe the evolution of the internal energy distribution of the stored ion ensemble. We find that significant heating of the electrosprayed ions occurs upon their extraction from the ion source, and that the radiative cooling rate is consistent with the prediction of a simple harmonic cascade model of vibrational relaxation.

DOI: 10.1103/PhysRevA.111.043112

I. INTRODUCTION

The discovery of green fluorescent protein (GFP) from the *Aequorea victoria* jellyfish was the cornerstone in the "green revolution" of biological fluorescence imaging and bio-engineering for the visualization of cellular processes [1,2]. The desirable optical properties of GFP and derivative fluorescent proteins and the ease with which they can be deployed as optical markers in biochemical systems has led to widespread use in life sciences [3,4]. These applications have spawned a field of study focused on the intrinsic photophysics and unimolecular reactions of the GFP chromophore, which determines the protein's optical properties. Many of these studies target the ionic forms of the bare chromophore isolated *in vacuo* [5–10], to avoid large solvatochromic effects [11]. In many cases, the gaseous ions have been shown to have similar absorption spectra to the protein [12], and they are small enough to be amenable to high-level theoretical calculations [13].

We present a study of the deprotonated anion of the chromophore of the cyan fluorescent protein (CFP, Fig. 1) [14], also called the W7 clone, a derivative of GFP that has found use in biological imaging. Compared to GFP, the CFP chromophore has an indole (tryptophan) moiety in place of the hydroxyphenyl (tyrosine) group. The photoresponse of this ion has been studied previously by Boyé *et al.* [15], who performed photodissociation action spectroscopy experiments using the electrostatic ion-beam storage ring ELISA [16]. They measured an absorption band maximum around 460 nm (2.7 eV), and modeled the rate coefficient for the dissociation process monitored in the action spectroscopy experiments. More recently, Fielding and co-workers used photoelectron spectroscopy to determine the anion's vertical detachment energy to be 2.75(2) eV, and they identified thermionic electron emission as an important decay mechanism for ions excited with photon energies from 3.5 to 4.0 eV [17,18]. The existence of thermionic emission, similar to the GFP chromophore [19], implies efficient recovery of the ground electronic state of the anion through internal conversion. Several of the present authors have investigated protonated cations of the cyan chromophore using photodissociation action spectroscopy, highlighting that multiple protonation isomers (protomers) may be generated in the gas phase [20].

Here, we report a measurement of the radiative cooling rate of the deprotonated CFP chromophore anion, determined from the time evolution of the laser-induced dissociation rate. Our experimental method is similar to that of Boyé *et al.* [15]. However, our experiments make use of the cryogenically cooled ($\approx$13 K) electrostatic ion-beam storage ring DESIREE [21,22]. Compared to ELISA, which operates at room temperature, the lower temperature and pressure inside DESIREE

---

[*] Contact author: mark.stockett@fysik.su.se

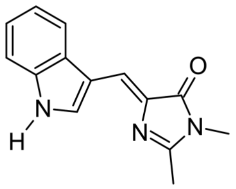

FIG. 1. Structure of the lowest energy conformation (Z-isomer) of the cyan fluorescent protein chromophore. Electrospray ionization deprotonates the NH group, generating the gas-phase anion.

enable studies of unimolecular processes on much longer timescales [23,24], up to hundreds of seconds [25]. Previous studies of radiative cooling rates measured at DESIREE have used sputtering or electron impact ion sources, which result in a high degree of internal excitation of the ions. Here, we report the use of an electrospray ionization (ESI) source in combination with DESIREE. ESI is a technique developed for transferring delicate biomolecular ions into the gas phase [26], but which delivers ion beam currents orders of magnitude lower than sources of atomic and cluster ions. To increase the stored ion beam current, ions produced by ESI are accumulated in an ion trap prior to injection into the DESIREE storage ring. Extraction of ions from the trap leads to collisions with background gas, resulting in heating of some fraction of the ion bunch. The relaxation of the ensemble by radiative cooling is monitored on the millisecond timescale, through quenching of the dissociation rate of collisionally activated ions, and on the second timescale through time-resolved laser-induced excitation.

II. METHODS

A. Ion production

The CFP chromophore [(5Z)-5-(1H-Indol-3-ylmethylene)-2,3-dimethyl-3,5-dihydro-4H-imidazol-4-one] was synthesized as part of a previous experiment [20]. The chromophore may exist in E and Z isomers about the methylene bond, with Z (shown in Fig. 1) being the lowest energy form. Because the synthesis was stereospecific for the Z isomer, as confirmed by NMR spectroscopy and x-ray crystallography [20], we expect the Z isomer to be the dominant gas-phase species. The existence of two geometric isomers is common to the GFP chromophore anion, which similarly has the Z isomer as the lowest energy form. Ion mobility experiments on the GFP chromophore anion have illustrated that the (synthesized) Z-isomer is the predominant gas-phase form [8].

The home-built ESI source used in this work has been described previously [27,28] and is illustrated in Fig. 2. Anions were sprayed from a solution containing the target compound dissolved in a 50:50 mixture of water and methanol with 5% by mass sodium hydroxide. A similar preparation was used by Boyé *et al.* [15]. All ions passing the heated capillary and ion funnel were accumulated in an octupole trap. The trap was emptied by pulsing the voltage on the exit lens to below the bias potential of the rods (pulse duration 1 ms), while simultaneously applying a −200 V pulse to tapered ejection electrodes interspersed with the rods [27,29]. The T-shaped ejection electrodes, shown in Fig. 2, were built following the design of Taban *et al.* [29] According to SIMION simulation performed by those authors, a 200 V potential applied to the tapered electrodes generates a nearly linear potential gradient on the order of 0.1 V/cm along the axis of the trap, which is 18 cm long [29]. This potential gradient temporally focuses the extracted ion bunch, leading to a peak in the front of the bunch profile with a width on the order of 100 μs. This width is comparable to the revolution period of ions in DESIREE, resulting in a higher number of stored ions compared to a continuous beam or a bunch extracted from the trap without use of ejection electrodes. Use of the ejection electrodes, however, results in heating the ions through energetic collisions with background gas in the trap (typical pressure $\sim 10^{-3}$ mbar). The ion bunches traveled through differentially pumped vacuum stages containing an octupole ion guide and a quadruple mass filter (operated with the mass-resolving DC voltage disabled), and were then accelerated to 34 keV. Ions with $m/z = 238$ were selected with a bending magnet and transported to the DESIREE ion-beam storage ring.

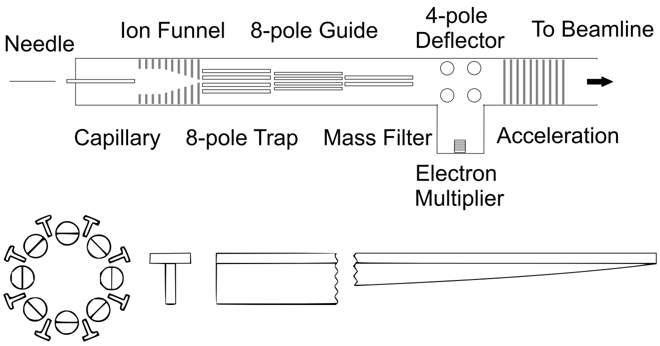

FIG. 2. Above: DESIREE electrospray ion source [27]. Ions are accumulated in the octupole trap, and bunches of ions extracted from the trap pass through the remaining sections to the experiment. Below: End view of the octupole accumulation trap with T-shaped ejection electrodes, and profiles of tapered T-shaped electrodes.

B. Storage ring experiments

The DESIREE ion-beam storage ring [21,22] used in the present experiments is shown in Fig. 3. Upon entering the storage ring, some of the ions may retain sufficient internal energy, acquired in collisions when exiting the octupole trap, to undergo unimolecular dissociation. Neutral fragments

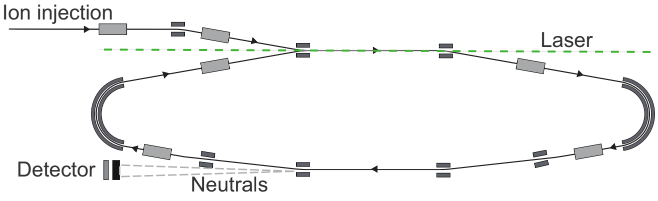

FIG. 3. Schematic of DESIREE ion-beam storage ring [21,22]. Ion beams (arrows) are guided by electrostatic ion optics (blocks) in a 13 K, extreme high vacuum environment. Neutral fragments emitted in the lower straight section are detected with a microchannel plate. Laser light is overlapped collinearly with the ion beam in the upper straight section.

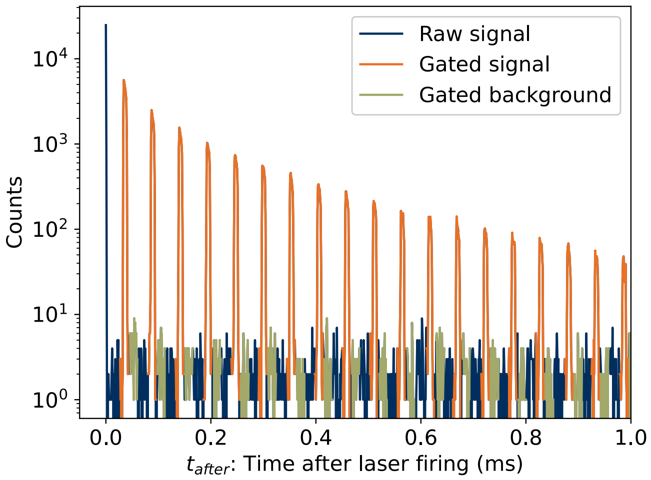

FIG. 4. Example of laser-induced dissociation signal from stored CFP chromophore anions. The narrow spike at $t_{\text{after}} = 0$ is due to scattered laser light. The subsequent peaks, highlighted in orange, are neutral counts due to laser-induced dissociation. The background windows are highlighted in green.

emitted in the observation arm of the storage ring (lower straight section in Fig. 3) are counted by a microchannel plate detector. This "spontaneous" collision-induced dissociation signal vanishes after about 100 ms, though most of the ions, having internal energies too low to dissociate, remain stored.

An optical parametric oscillator system (Ekspla NT232C) was used to generate laser light at 435 nm (2.85 eV). Laser pulses of ~5 ns duration and 3.6 mJ average energy (measured after the light passed through the vacuum chamber) were overlapped collinearly with the stored ion beam in the excitation arm of the storage ring (upper straight section in Fig. 3) at a 10 Hz repetition rate. Note that the laser beam interacts with only about 10% of the ion bunch, which is spread around nearly the full circumference of the storage ring. As in the spontaneous dissociation measurements, neutrals are collected from the observation arm on the opposite side of the storage ring. In postprocessing, the laser-induced signal was gated in time, and the counts in a background gate were subtracted, as illustrated in Fig. 4.

C. Kinetic model

Our approach to kinetic modeling of unimolecular dissociation and vibrational radiative cooling has been described previously [30,31]. The vibrational frequencies and infrared intensities of the CFP chromophore anion were calculated at the LC-ωHPBE/aug-cc-pVTZ level [32,33] in GAUSSIAN 16 [34]. The vibrational emission rate coefficients were computed using the simple harmonic cascade (SHC) approximation [35]:

$$k_{\text{rad},s}(E) = A_s \sum_{v=1}^{v \leqslant E/h\nu_s} \frac{\rho(E - vh\nu_s)}{\rho(E)}, \tag{1}$$

where E is the total internal energy, v is the vibrational quantum number, and $h\nu_s$ and A_s are the transition energy and Einstein coefficient of vibrational mode s, respectively. The density of vibrational states $\rho(E)$ was calculated using the Beyer-Swinehart algorithm [36]. The SHC model considers only $v \rightarrow v - 1$ fundamental transitions. The total radiative cooling rate coefficient is $k_{\text{rad}}(E) = \sum_s k_{\text{rad},s}(E)$.

The dissociation rate coefficient is modeled using the microcanonical expression

$$k_{\text{diss}}(E) = A_{\text{diss}} \frac{\rho(E - E_{\text{diss}})}{\rho(E)}, \tag{2}$$

where $A_{\text{diss}} = 1 \times 10^{13}\ \text{s}^{-1}$ is the frequency factor, and $E_{\text{diss}} = 1.6$ eV is the dissociation energy. The numerical values of these parameters were adopted from the previous measurements of the CFP chromophore anion by Boyé *et al.* [15]. We do not expect thermionic electron emission to be competitive in our experiments, given that the activation energy (the electron affinity, calculated to be 2.67 eV [17]) is much higher than E_{diss}.

The time evolution of the internal energy distribution $g(E, t)$ of the ensemble is given by the master equation:

$$\begin{aligned} \frac{d}{dt} g(E, t) = &- k_{\text{diss}}(E) g(E, t) \\ &+ \sum_s [k_{\text{rad},s}(E + h\nu_s) g(E + h\nu_s, t) \\ &- k_{\text{rad},s}(E) g(E, t)]. \end{aligned} \tag{3}$$

The first term gives the depletion of the population by unimolecular dissociation. The first term in brackets represents $v + 1 \rightarrow v$ vibrational emission from levels above E, while the second is $v \rightarrow v - 1$ emission to levels below E. The time step dt is chosen to match the experimental data, with 32 additional, equally spaced points prior to the first experimental time bin to account for ion decays during the transit time from the ion source to the storage ring. For simplicity, the initial energy distribution $g(E, 0)$ is assumed to follow Boltzmann statistics. Note that this model implicitly assumes that intramolecular vibrational redistribution occurs much more rapidly than dissociation or vibrational relaxation. The simulated dissociation rate is given by

$$R_{\text{sim}}(t) = \int k_{\text{diss}}(E) g(E, t) dE. \tag{4}$$

III. RESULTS AND DISCUSSION

A. Collisionally activated dissociation

The measured count rate $R(t)$ of neutral fragments emitted from stored CFP chromophore anions is shown in Fig. 5. The dissociating ions are presumably heated in collisions with background gas when extracted from the octupole ion trap. The broad internal energy distribution of the collisionally excited ions gives rise to the characteristic power-law time dependence [37] of the dissociation rate $R(t) \propto t^{-1}$. After about 10 ms, radiative cooling becomes competitive with dissociation, and the count rate is quenched [38]. After about 50 ms, a constant count rate is reached, which is mainly the detector dark rate. The signal, after subtraction of this background count rate, is modeled with the expression

$$R(t) = r_0 t^{-1} e^{-k_c t}, \tag{5}$$

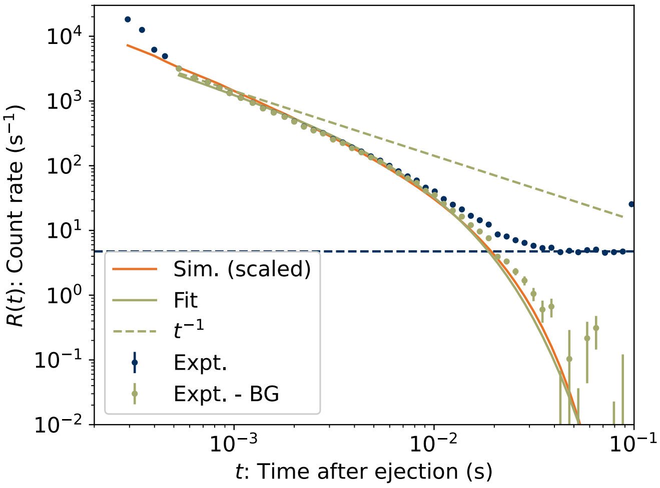

FIG. 5. Neutral yield measured from a stored CFP chromophore anion beam due to collisionally activated dissociation. The dashed line indicates the background (BG) count rate, and "Expt-BG" is the experimental data with this background subtracted.

where r_0 is a dimensionless normalization constant, and k_c is the critical rate coefficient which characterizes the radiative cooling process. A fit of Eq. (5) to the background-subtracted count rate returned $k_c = 148(6)$ s^{-1}. Values of k_c on the order of 100 s^{-1} are typical of vibrational (infrared) radiative cooling. The rapid decline in the count rate in the first few turns is likely due to the loss of circulating ions having velocities outside the acceptance of the storage ring. The time focusing effect of the ejection electrodes likely contributes to this effect by increasing the velocity spread of the ion bunch. The points corresponding to the first four revolutions of the ion beam in the storage ring are excluded from the fit.

A master equation simulation (Sec. II C) reproduces the measured dissociation rate satisfactorily. The simulation shown in Fig. 5 was initialized to a Boltzmann distribution with a temperature of 1000 K and reproduces the shape of the measured decay rate curve. The choice of initial temperature primarily affects the overall magnitude of the simulated dissociation rate. As the number of stored ions in the experiment is too low to be measured with existing diagnostics, no robust comparison of the absolute magnitudes is possible, and the initial temperature used in the simulation should be considered an order-of-magnitude estimate. Both the fit of Eq. (5) and the master equation simulation underestimate the measured dissociation rate after about 25 ms. This is not unusual for such simplified statistical models [31,39].

The rate coefficients for dissociation and vibrational radiative cooling used in the simulation are plotted in Fig. 6. The value of k_c determined from the fit of Eq. (5) is plotted as a horizontal line. The value of the calculated dissociation and radiative rate coefficients at the point where they cross is within 20% of the measured value of k_c, which is typical of the accuracy of the simple harmonic cascade model [30,40]. The dashed vertical line in Fig 6 indicates the 2.85 eV photon energy used in the laser experiment.

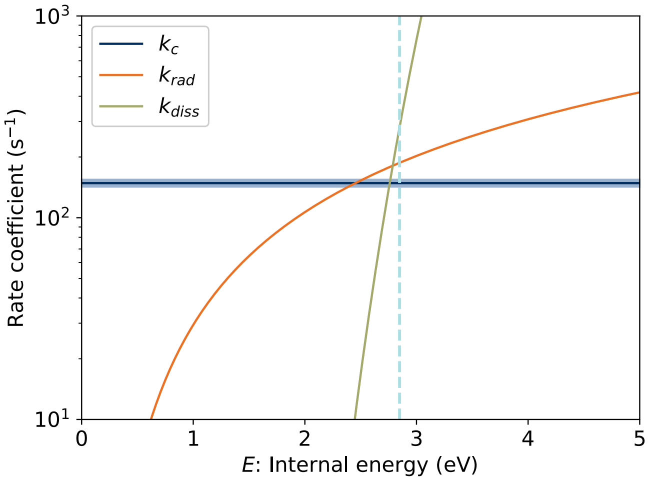

FIG. 6. Rate coefficients for vibrational radiative cooling [Eq. (1)] and dissociation [Eq. (2)]. The horizontal line shows the value of k_c obtained from the spontaneous decay measurement (Fig. 5), while the vertical dashed line indicates the photon energy used in the laser experiment.

Our measurement is sensitive only to ions with internal energies within a narrow window given by the timescale of the experiment. Ions with energies significantly above 3.2 eV will dissociate with rate coefficients greater than 2000 s^{-1}, i.e., before the first measured point in Fig. 5. Ions with energies below 2.8 eV will have dissociation rate coefficients below k_c and thus be more likely to be stabilized by radiative cooling. Any initial energy distribution $g(E, 0)$ that is broad compared to this energy window will result in a rate curve given by Eq. (5).

B. Laser-induced dissociation

Examples of the laser-induced dissociation rate $R_e(t)$ for different laser firing times t_{laser}, measured from the time injection, are given in Fig. 7. The time t_{after} is measured from the laser firing time. The time dependence of the dissociation rate is nonexponential, which could imply contributions from multiple-photon processes. However, according to our kinetic

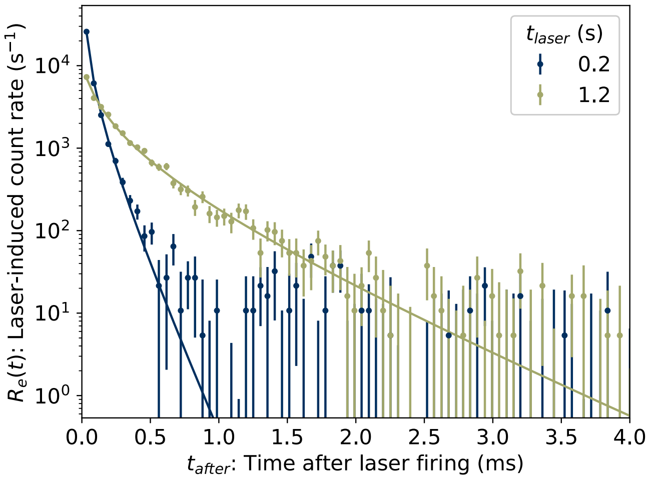

FIG. 7. Examples of the laser-induced dissociation rate of CFP chromophore anions excited by 2.85 eV photons at different laser firing times t_{laser}. The solid lines are fits of Eq. (6).

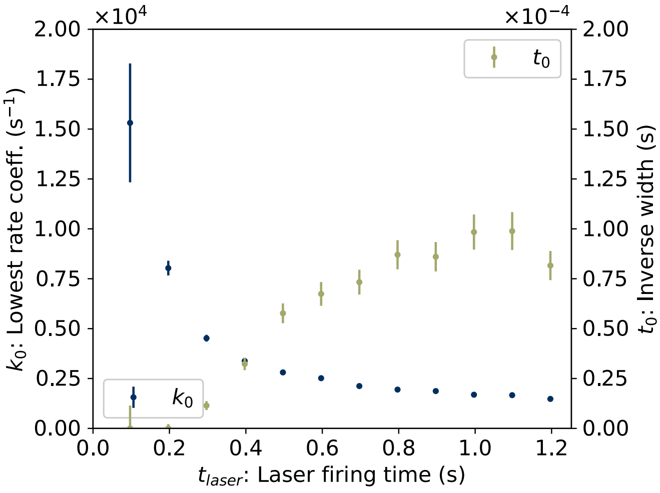

FIG. 8. Parameters k_0 and t_0 from fits of Eq. (6) to laser-induced dissociation rates of CFP chromophore anions.

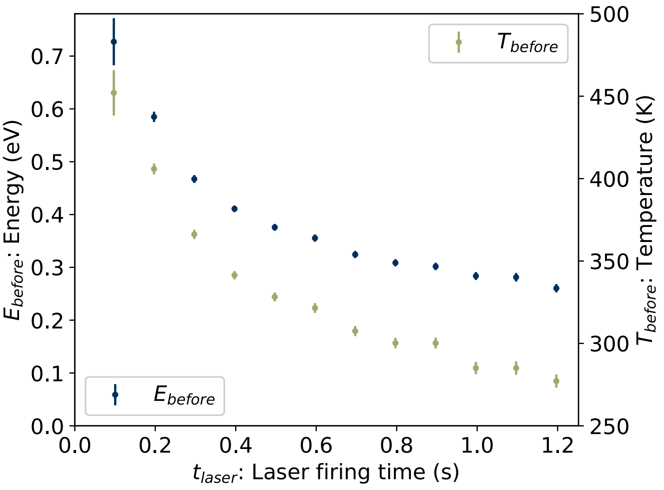

FIG. 9. Microcanonical energy E_{before} and equivalent temperature T_{before} of CFP chromophore anions prior to laser excitation.

model, ions absorbing two 2.85 eV photons would dissociate with a rate coefficient not less than 6×10^6 s^{-1}. Such highly excited ions would dissociate within the tens of μs required for transport between the excitation and observation arms of the storage ring (see Fig. 3) and thus not contribute to the measured $R_e(t)$. We thus attribute the nonexponential time dependence to the distribution of internal energies of the ions prior to laser excitation. The solid lines are fits of the expression

$$R_e(t_{\text{after}}) = r_0(t_{\text{after}} + t_0)^{-1}e^{-k_0(t_{\text{after}}+t_0)}, \tag{6}$$

which is simply a time-shifted version of Eq. (5). In experiments where the laser photon energy $h\nu$ is well below the destruction threshold, Eq. (6) has been used, assuming a constant value of $k_0 = k_c$ taken from spontaneous decay measurements like those in Fig. 5, to determine the radiative cooling rate by connecting the typical energy of the ion ensemble before and after photon absorption to the time difference $t_{\text{laser}} - t_0$ [30,41–43]. In the present case, where the photon energy is significantly above the crossing point where radiative cooling is competitive (see Fig. 6), absorption of a single photon will always shift the entire energy distribution into the dissociation-dominated regime. We take k_0 as a fit parameter corresponding to the dissociation rate coefficient of the ions in the ensemble with the lowest internal energy, with t_0 characterizing the width of the distribution. The fitted values of k_0 and t_0 are plotted in Fig. 8. At the largest laser firing times, the fitted k_0 values are an order of magnitude greater than k_c, confirming that even the coldest ions are excited to well above the crossing point. According to the rate coefficients in Fig. 6, an ion decaying with a total rate coefficient of 1500 s^{-1} will dissociate nearly 90% of the time.

In general, the observed dissociation rate is the ensemble average of the dissociation rate coefficient:

$$R(t) \propto \int k_{\text{diss}}(E)g(E,t)dE, \tag{7}$$

where $g(E,t)$ is the internal energy distribution of the ion ensemble. Given that isolated ions with energy E will decay with a characteristic lifetime given by $k_{\text{diss}}(E)^{-1}$, Eq. (7) can be recast as a weighted sum of decay rates:

$$R(t) \propto \int \mathcal{F}(k_{\text{diss}})e^{-k_{\text{diss}}t}dk_{\text{diss}}, \tag{8}$$

where $\mathcal{F}(k_{\text{diss}})$ is called the rate weighting function [44], and it is the inverse Laplace transform of $R(t)$. Our model for the laser-induced dissociation rate in Eq. (6) is the Laplace transform of

$$\mathcal{F}(k_{\text{diss}}) = u(k_{\text{diss}} - k_0)e^{-(k_{\text{diss}}-k_0)t_0}, \tag{9}$$

where $u(k)$ is the Heaviside step function. In the present situation, where all of the photoexcited ions have internal energies making radiative cooling noncompetitive, the energy distribution after photon absorption $g(E, t_{\text{after}}) \approx g(E, t_{\text{after}} = 0)e^{-k_{\text{diss}}t_{\text{after}}}$. With a simple change of variables, we obtain [44]

$$g(E, t_{\text{after}} = 0) = \mathcal{F}(k_{\text{diss}}(E))\frac{d}{dE}\log(k_{\text{diss}}(E)). \tag{10}$$

For an Arrhenius-type dissociation rate coefficient, the factor $\frac{d}{dE}\log(k_{\text{diss}}(E)) \propto E^{-2}$.

From Eqs. (9) and (10), we find that the laser-induced dissociation rate is dominated by ions with internal energies E_m where $k_{\text{diss}}(E_m) = k_0$. We can thus use k_0 as a thermometer to probe the time evolution of the energy distribution of the stored ion ensemble. For each value of k_0, we determine a value of E_m from the model dissociation rate coefficient [Eq. (2)]. Subtracting the photon energy $h\nu$ gives the typical energy of the stored ions before absorption, $E_{\text{before}} = E_m - h\nu$. This microcanonical energy can be related to a temperature using the caloric curve defined by

$$\frac{1}{k_BT} = \frac{d}{dE}\log\rho(E). \tag{11}$$

The resulting energies E_{before} and temperatures T_{before} are plotted in Fig. 9. Evidently, the use of ejection electrodes increases the typical internal energies of the injected ions above that of the laboratory environment (≈300 K).

Extrapolation of these results indicates that hundreds of seconds would be needed for the CFP chromophore anion to cool to the ambient temperature of DESIREE by radiative

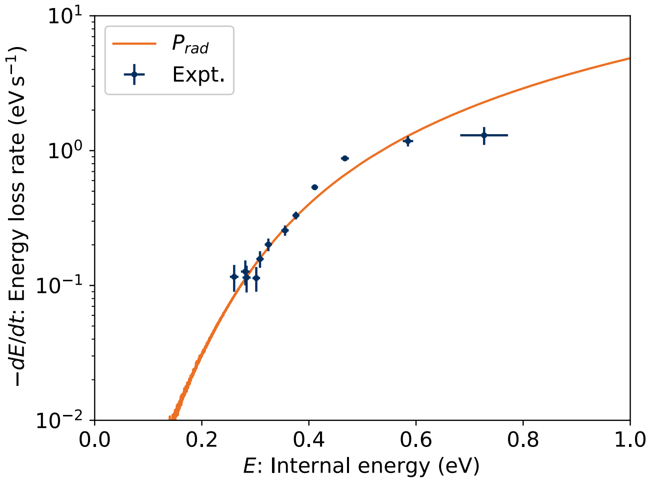

FIG. 10. Measured energy loss rate of CFP chromophore anions compared to the total radiative power P_{rad} from the SHC model.

cooling alone. The DESIREE ESI source is equipped with a cryogenic ring-electrode trap [27,45] for precooling ions prior to injection. This trap will be implemented in future experiments. Such a combination of a cryogenic ion trap with an electrostatic ion-beam storage ring has been realized at SAPHIRA [46], enabling, e.g., high-resolution spectroscopy of the GFP chromophore [10].

Our approach to analyzing the laser-induced decay rates is very similar to that of Rasmussen *et al.* [47], with a few technical distinctions. Rasmussen *et al.* fit a single exponential function to their laser-induced decay rates, corresponding to $\mathcal{F}(k) = \delta(k - k_0)$. Our model [Eq. (6)] accounts for the finite width of the energy distribution and better fits the data at short times after laser firing (cf., Ref. [47], Fig. 3c). Due to the 300 K ambient temperature inside the ELISA storage ring used in Rasmussen's measurements, compared to 13 K for DESIREE, their background count rate is much higher and is treated as a fit parameter. Here, we subtract a measured background rate prior to fitting (see Fig. 4).

The rate of change in the microcanonical energy prior to laser excitation, $dE/dt \equiv dE_{\mathrm{before}}/dt_{\mathrm{laser}}$, may be compared to the total radiative power $P_{\mathrm{rad}} = \sum_s k_{\mathrm{rad},s} h\nu_s$, as shown in Fig. 10. The agreement between theory and experiment is once again satisfactory. If we consider the accuracy of our model for the dissociation and radiative cooling rate coefficients to be demonstrated by the collisionally activated dissociation experiment (Sec. III A), this result validates our approach to the analysis connecting the time-resolved laser-induced dissociation rates to the internal energy distribution of the stored ion ensemble.

IV. CONCLUSIONS

An electrospray ion source has been coupled to the DESIREE electrostatic ion-beam storage ring. The use of an octupole ion trap equipped with ejection electrodes to intensify the ion bunches injected into the DESIREE storage ring results in significant heating of the ions. The stored ion ensemble relaxes by radiative cooling to below room temperature within 1 s. The radiative cooling rate of the deprotonated cyan fluorescent protein chromophore anion has been shown to be consistent with predictions from a simple harmonic cascade model of vibrational relaxation. Future developments will include the implementation of a cryogenically cooled ring-electrode ion trap to precool electrosprayed ions prior to injection.

ACKNOWLEDGMENTS

This work was supported by Swedish Research Council Grants No. 2016-03675 (M.H.S.), No. 2018-04092 (H.T.S.), No. 2023-03833 (H.C.), No. 2020-03437 (H.Z.), Knut and Alice Wallenberg Foundation Grant No. 2018.0028 (H.C., H.T.S., and H.Z.), EPSRC Grant No. EP/W018691 (J.N.B.), Olle Engkvist Foundation Grant No. 200-575 (M.H.S.), and Swedish Foundation for International Collaboration in Research and Higher Education (STINT) Grant No. PT2017-7328 (J.N.B. and M.H.S.). We acknowledge the DESIREE infrastructure for the provision of facilities and experimental support, and we thank the operators and technical staff for their invaluable assistance. The DESIREE infrastructure receives funding from the Swedish Research Council under Grants No. 2021-00155 and No. 2023-00170. This article is based upon work from COST Action CA21126–Carbon molecular nanostructures in space (NanoSpace), supported by COST (European Cooperation in Science and Technology).

APPENDIX

Figure 11 shows the density of vibrational states computed from the vibrational frequencies in Table I.

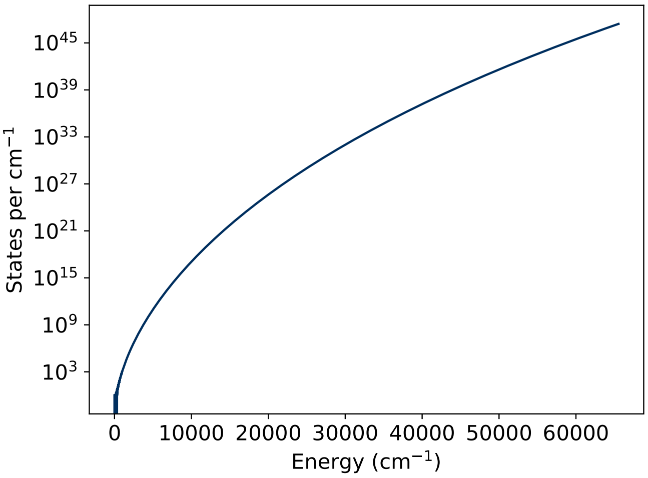

FIG. 11. Density of vibrational states computed from the vibrational frequencies in Table I using the Beyer-Swinehart algorithm.

TABLE I. Vibrational frequencies and IR intensities of the CFP chromophore anion computed at the LC-ωHPBE/aug-cc-pVTZ level.

Mode	Frequency (cm^{-1})	Intensity (km/mol)
1	41.6481	0.0778
2	53.5582	0.7942
3	75.1929	0.5335
4	102.5178	0.7561
5	125.6250	2.2210
6	153.2787	0.0720
7	167.1570	2.2075
8	183.1901	0.1856
9	202.5202	0.5531
10	228.4538	6.7832
11	250.6966	3.9834
12	266.1896	2.8475
13	276.2275	4.1583
14	329.6837	4.6192
15	366.3549	1.1828
16	448.8581	5.0564
17	448.9690	6.7444
18	508.1362	0.0258
19	538.7693	10.9615
20	584.1953	54.8102
21	605.6492	17.3971
22	619.4859	0.1029
23	623.4400	39.4952
24	660.5806	0.7453
25	686.0771	3.5060
26	725.4207	14.5641
27	761.6796	76.8140
28	763.6519	21.9483
29	780.2185	7.1314
30	782.1671	1.6423
31	812.1580	0.5767
32	817.8358	100.9934
33	880.8038	0.2758
34	889.2496	21.5884
35	921.7655	3.9908
36	940.4976	80.3746
37	962.2362	3.1329
38	986.5221	6.1541
39	1013.6131	7.0102
40	1025.9570	1.0785
41	1040.6908	20.8248
42	1047.4820	1.2660
43	1056.8460	29.0533
44	1105.7116	15.2428
45	1133.4593	266.4592
46	1147.8793	0.5226
47	1160.2312	106.6973
48	1173.7230	164.0179
49	1201.4520	23.5901
50	1229.7879	36.5877
51	1257.5610	241.4628
52	1301.0785	202.8437
53	1340.1625	56.5201
54	1350.4369	138.9834
55	1380.3360	40.1796
56	1384.9824	144.2089
57	1396.7129	139.7355
58	1413.5822	17.8570
59	1444.3583	519.3765
60	1456.0541	90.7845
61	1461.4857	3.5596
62	1485.6896	10.5412
63	1489.0096	31.6475
64	1492.0066	44.2745
65	1503.0598	185.5949
66	1517.6926	57.5845
67	1538.1043	514.4644
68	1624.1768	937.1899
69	1632.0424	454.4385
70	1672.6515	214.4911
71	1685.2334	676.4360
72	1740.4363	319.8310
73	3022.4700	71.1798
74	3027.8638	176.5195
75	3084.9569	11.6740
76	3087.3866	54.8054
77	3143.3162	2.2671
78	3147.2846	6.0313
79	3160.3150	6.6709
80	3162.7258	10.0081
81	3169.2890	37.1379
82	3179.4200	43.4069
83	3194.9292	65.2400
84	3219.5058	16.9875

[1] M. Chalfie, Y. Tu, G. Euskirchen, W. W. Ward, and D. C. Prasher, Green fluorescent protein as a marker for gene expression, Science **263**, 802 (1994).

[2] R. Y. Tsien, The green fluorescent protein, Annu. Rev. Biochem. **67**, 509 (1998).

[3] N. C. Shaner, P. A. Steinbach, and R. Y. Tsien, A guide to choosing fluorescent proteins, Nat. Methods **2**, 905 (2005).

[4] A. S. Mishin, V. V. Belousov, K. M. Solntsev, and K. A. Lukyanov, Novel uses of fluorescent proteins, Curr. Opin. Chem. Biol. **27**, 1 (2015).

[5] L. H. Andersen, H. Bluhme, S. Boyé, T. J. D. Jørgensen, H. Krogh, I. B. Nielsen, S. Brøndsted Nielsen, and A. Svendsen, Experimental studies of the photophysics of gas-phase fluorescent protein chromophores, Phys. Chem. Chem. Phys. **6**, 2617 (2004).

[6] M. W. Forbes and R. A. Jockusch, Deactivation pathways of an isolated green fluorescent protein model chromophore studied by electronic action spectroscopy, J. Am. Chem. Soc. **131**, 17038 (2009).

[7] A. Svendsen, H. V. Kiefer, H. B. Pedersen, A. V. Bochenkova, and L. H. Andersen, Origin of the intrinsic fluorescence of the green fluorescent protein, J. Am. Chem. Soc. **139**, 8766 (2017).

[8] E. Carrascosa, J. N. Bull, M. S. Scholz, N. J. A. Coughlan, S. Olsen, U. Wille, and E. J. Bieske, Reversible photoisomer-

ization of the isolated green fluorescent protein chromophore, J. Phys. Chem. Lett. **9**, 2647 (2018).

[9] W. Zagorec-Marks, M. M. Foreman, J. R. R. Verlet, and J. M. Weber, Cryogenic ion spectroscopy of the green fluorescent protein chromophore in vacuo, J. Phys. Chem. Lett. **10**, 7817 (2019).

[10] L. H. Andersen, A. P. Rasmussen, H. B. Pedersen, O. B. Beletsan, and A. V. Bochenkova, High-resolution spectroscopy and selective photoresponse of cryogenically cooled green fluorescent protein chromophore anions, J. Phys. Chem. Lett. **14**, 6395 (2023).

[11] E. K. Ashworth, M.-H. Kao, C. S. Anstöter, G. Riesco-Llach, L. Blancafort, K. M. Solntsev, S. R. Meech, J. R. R. Verlet, and J. N. Bull, Alkylated green fluorescent protein chromophores: dynamics in the gas phase and in aqueous solution, Phys. Chem. Chem. Phys. **25**, 23626 (2023).

[12] S. B. Nielsen, A. Lapierre, J. U. Andersen, U. V. Pedersen, S. Tomita, and L. H. Andersen, Absorption spectrum of the green fluorescent protein chromophore anion in vacuo, Phys. Rev. Lett. **87**, 228102 (2001).

[13] N. H. List, C. M. Jones, and T. J. Martínez, Internal conversion of the anionic gfp chromophore: in and out of the i-twisted S_1/S_0 conical intersection seam, Chem. Sci. **13**, 373 (2022).

[14] R. Heim, D. C. Prasher, and R. Y. Tsien, Wavelength mutations and posttranslational autoxidation of green fluorescent protein, Proc. Natl. Acad. Sci. USA **91**, 12501 (1994).

[15] S. Boyé, I. B. Nielsen, S. B. Nielsen, H. Krogh, A. Lapierre, H. B. Pedersen, S. U. Pedersen, U. V. Pedersen, and L. H. Andersen, Gas-phase absorption properties of a green fluorescent protein-mutant chromophore: The W7 clone, J. Chem. Phys. **119**, 338 (2003).

[16] J. U. Andersen, P. Hvelplund, S. B. Nielsen, S. Tomita, H. Wahlgreen, S. P. Møller, U. V. Pedersen, J. S. Forster, and T. J. D. Jørgensen, The combination of an electrospray ion source and an electrostatic storage ring for lifetime and spectroscopy experiments on biomolecules, Rev. Sci. Instrum. **73**, 1284 (2002).

[17] M. A. Parkes, A. Bennett, and H. H. Fielding, A photoelectron imaging and quantum chemistry study of the deprotonated cyan fluorescent protein chromophore anion, Mol. Phys. **117**, 3027 (2019).

[18] C. R. S. Mooney, M. E. Sanz, A. R. McKay, R. J. Fitzmaurice, A. E. Aliev, S. Caddick, and H. H. Fielding, Photodetachment spectra of deprotonated fluorescent protein chromophore anions, J. Phys. Chem. A **116**, 7943 (2012).

[19] C. W. West, J. N. Bull, A. S. Hudson, S. L. Cobb, and J. R. R. Verlet, Excited state dynamics of the isolated green fluorescent protein chromophore anion following UV excitation, J. Phys. Chem. B **119**, 3982 (2015).

[20] E. K. Ashworth, J. Dezalay, C. Ryan, C. Ieritano, S. Hopkins, I. Chambrier, A. N. Cammidge, M. H. Stockett, J. A. Noble, and J. N. Bull, Protomers of the green and cyan fluorescent protein chromophores investigated using action spectroscopy, Phys. Chem. Chem. Phys. **25**, 20405 (2023).

[21] R. D. Thomas, H. T. Schmidt, G. Andler, M. Björkhage, M. Blom, L. Brännholm, E. Bäckström, H. Danared, S. Das, N. Haag, P. Halldén, F. Hellberg, A. I. S. Holm, H. A. B. Johansson, A. Källberg, G. Källersjö, M. Larsson, S. Leontein, L. Liljeby, P. Löfgren, B. Malm, S. Mannervik, M. Masuda, D. Misra, A. Orbán, A. Paál, P. Reinhed, K.-G. Rensfelt, S. Rosén, K. Schmidt, F. Seitz, A. Simonsson, J. Weimer, H. Zettergren, and H. Cederquist, The double electrostatic ion ring experiment: A unique cryogenic electrostatic storage ring for merged ion-beams studies, Rev. Sci. Instrum. **82**, 065112 (2011).

[22] H. T. Schmidt, R. D. Thomas, M. Gatchell, S. Rosén, P. Reinhed, P. Löfgren, L. Brännholm, M. Blom, M. Björkhage, E. Bäckström, J. D. Alexander, S. Leontein, D. Hanstorp, H. Zettergren, L. Liljeby, A. Källberg, A. Simonsson, F. Hellberg, S. Mannervik, M. Larsson, W. D. Geppert, K. G. Rensfelt, H. Danared, A. Paál, M. Masuda, P. Halldén, G. Andler, M. H. Stockett, T. Chen, G. Källersjö, J. Weimer, K. Hansen, H. Hartman, and H. Cederquist, First storage of ion beams in the Double Electrostatic Ion-Ring ExpEriment: DESIREE, Rev. Sci. Instrum. **84**, 055115 (2013).

[23] J. N. Bull, M. S. Scholz, E. Carrascosa, M. K. Kristiansson, G. Eklund, N. Punnakayathil, N. de Ruette, H. Zettergren, H. T. Schmidt, H. Cederquist, and M. H. Stockett, Ultraslow radiative cooling of C_n^- ($n = 3 - 5$), J. Chem. Phys. **151**, 114304 (2019).

[24] M. H. Stockett, M. Björkhage, H. Cederquist, H. Schmidt, and H. Zettergren, Storage time dependent photodissociation action spectroscopy of polycyclic aromatic hydrocarbon cations in the cryogenic electrostatic storage ring DESIREE, Faraday Discuss. **217**, 126 (2019).

[25] H. T. Schmidt, G. Eklund, K. C. Chartkunchand, E. K. Anderson, M. Kamińska, N. de Ruette, R. D. Thomas, M. K. Kristiansson, M. Gatchell, P. Reinhed, S. Rosén, A. Simonsson, A. Källberg, P. Löfgren, S. Mannervik, H. Zettergren, and H. Cederquist, Rotationally cold OH^- ions in the cryogenic electrostatic ion-beam storage ring DESIREE, Phys. Rev. Lett. **119**, 073001 (2017).

[26] J. B. Fenn, M. Mann, C. K. Meng, S. F. Wong, and C. M. Whitehouse, Electrospray ionization for mass spectrometry of large biomolecules, Science **246**, 64 (1989).

[27] N. de Ruette, M. Wolf, L. Giacomozzi, J. D. Alexander, M. Gatchell, M. H. Stockett, N. Haag, H. Zettergren, H. T. Schmidt, and H. Cederquist, DESIREE electrospray ion source test bench and setup for collision induced dissociation experiments, Rev. Sci. Instrum. **89**, 075102 (2018).

[28] M. H. Stockett, M. Gatchell, J. D. Alexander, U. Berzins, T. Chen, K. Farid, A. Johansson, K. Kulyk, P. Rousseau, K. Støchkel, L. Adoui, P. Hvelplund, B. A. Huber, H. T. Schmidt, H. Zettergren, and H. Cederquist, Fragmentation of anthracene $C_{14}H_{10}$, acridine $C_{13}H_9N$ and phenazine $C_{12}H_8N_2$ ions in collisions with atoms, Phys. Chem. Chem. Phys. **16**, 21980 (2014).

[29] I. M. Taban, L. A. McDonnell, A. Römpp, I. Cerjak, and R. M. A. Heeren, Simion analysis of a high performance linear accumulation octopole with enhanced ejection capabilities, Int. J. Mass Spectrom. **244**, 135 (2005).

[30] M. H. Stockett, J. N. Bull, J. T. Buntine, E. Carrascosa, M. Ji, N. Kono, H. T. Schmidt, and H. Zettergren, Unimolecular fragmentation and radiative cooling of isolated PAH ions: A quantitative study, J. Chem. Phys. **153**, 154303 (2020).

[31] M. H. Stockett, J. N. Bull, H. Cederquist, S. Indrajith, M. Ji, J. E. Navarro Navarrete, H. T. Schmidt, H. Zettergren, and B. Zhu, Efficient stabilization of cyanonaphthalene by fast radiative cooling and implications for the resilience of small pahs in interstellar clouds, Nat. Commun. **14**, 395 (2023).

[32] R. A. Kendall, T. H. Dunning, and R. J. Harrison, Electron affinities of the first-row atoms revisited. Systematic

basis sets and wave functions, J. Chem. Phys. **96**, 6796 (1992).

[33] T. M. Henderson, A. F. Izmaylov, G. Scalmani, and G. E. Scuseria, Can short-range hybrids describe long-range-dependent properties? J. Chem. Phys. **131**, 044108 (2009).

[34] M. J. Frisch, G. W. Trucks, H. B. Schlegel, G. E. Scuseria, M. A. Robb, J. R. Cheeseman, G. Scalmani, V. Barone, B. Mennucci, G. A. Petersson, H. Nakatsuji, M. Caricato, X. Li, H. P. Hratchian, A. F. Izmaylov, J. Bloino, G. Zheng, J. L. Sonnenberg, M. Hada, M. Ehara, K. Toyota, R. Fukuda, J. Hasegawa, M. Ishida, T. Nakajima, Y. Honda, O. Kitao, H. Nakai, T. Vreven, J. A. Montgomery, Jr., J. E. Peralta, F. Ogliaro, M. Bearpark, J. J. Heyd, E. Brothers, K. N. Kudin, V. N. Staroverov, R. Kobayashi, J. Normand, K. Raghavachari, A. Rendell, J. C. Burant, S. S. Iyengar, J. Tomasi, M. Cossi, N. Rega, J. M. Millam, M. Klene, J. E. Knox, J. B. Cross, V. Bakken, C. Adamo, J. Jaramillo, R. Gomperts, R. E. Stratmann, O. Yazyev, A. J. Austin, R. Cammi, C. Pomelli, J. W. Ochterski, R. L. Martin, K. Morokuma, V. G. Zakrzewski, G. A. Voth, P. Salvador, J. J. Dannenberg, S. Dapprich, A. D. Daniels, Ö. Farkas, J. B. Foresman, J. V. Ortiz, J. Cioslowski, and D. J. Fox, *Gaussian 16 Revision B.01* (Gaussian Inc., Wallingford, CT, 2016).

[35] K. Hansen, O. Licht, A. Kurbanov, and Y. Toker, Cascade infrared thermal photon emission, J. Phys. Chem. A **127**, 2889 (2023).

[36] T. Beyer and D. F. Swinehart, Algorithm 448: Number of multiply-restricted partitions, Commun. ACM **16**, 379 (1973).

[37] K. Hansen, J. U. Andersen, P. Hvelplund, S. P. Møller, U. V. Pedersen, and V. V. Petrunin, Observation of a 1/t decay law for hot clusters and molecules in a storage ring, Phys. Rev. Lett. **87**, 123401 (2001).

[38] J. Andersen, H. Cederquist, J. Forster, B. Huber, P. Hvelplund, J. Jensen, B. Liu, B. Manil, L. Maunoury, S. Brøndsted Nielsen, U. Pedersen, H. Schmidt, S. Tomita, and H. Zettergren, English Power-law decay of collisionally excited amino acids and quenching by radiative cooling, Euro. Phys. J. D **25**, 139 (2003).

[39] J. Bernard, M. Ji, S. Indrajith, M. H. Stockett, J. E. Navarro Navarrete, N. Kono, H. Cederquist, S. Martin, H. Schmidt, and H. Zettergren, Efficient radiative cooling of tetracene cations $C_{18}H_{12}^+$: absolute recurrent fluorescence rates as a function of internal energy, Phys. Chem. Chem. Phys. **25**, 10726 (2023).

[40] M. H. Stockett, J. N. Bull, J. T. Buntine, E. Carrascosa, E. K. Anderson, M. Gatchell, M. Kaminska, R. F. Nascimento, H. Cederquist, H. T. Schmidt, and H. Zettergren, Radiative cooling of carbon cluster anions C_{2n+1}^- ($n = 3 - 5$), Eur. Phys. J. D **74**, 150 (2020).

[41] A. E. K. Sundén, M. Goto, J. Matsumoto, H. Shiromaru, H. Tanuma, T. Azuma, J. U. Andersen, S. E. Canton, and K. Hansen, Absolute cooling rates of freely decaying fullerenes, Phys. Rev. Lett. **103**, 143001 (2009).

[42] K. Hansen, C_{60}^- thermal electron-emission rate, Phys. Rev. A **102**, 052823 (2020).

[43] J. E. Navarro Navarrete, J. N. Bull, H. Cederquist, S. Indrajith, M. Ji, H. Schmidt, H. Zettergren, B. Zhu, and M. H. Stockett, Experimental radiative cooling rates of a polycyclic aromatic hydrocarbon cation, Faraday Discuss. **245**, 352 (2023).

[44] B. Zhu, J. N. Bull, M. Ji, H. Zettergren, and M. H. Stockett, Radiative cooling rates of substituted PAH ions, J. Chem. Phys. **157**, 044303 (2022).

[45] A. Luca, S. Schlemmer, I. Čermák, and D. Gerlich, On the combination of a linear field free trap with a time-of-flight mass spectrometer, Rev. Sci. Instrum. **72**, 2900 (2001).

[46] H. B. Pedersen, H. Juul, F. K. Mikkelsen, A. P. Rasmussen, and L. H. Andersen, Inline cryogenically cooled radio-frequency ion trap as a universal injector for cold ions into an electrostatic ion-beam storage ring: Probing and modeling the dynamics of rotational cooling of OH^-, Phys. Rev. A **106**, 053111 (2022).

[47] A. P. Rasmussen, R. Teiwes, D. A. Farkhutdinova, A. V. Bochenkova, and L. H. Andersen, On the temperature of large biomolecules in ion-storage rings, Eur. Phys. J. D **76**, 76 (2022).